Cite this: *Nanoscale*, 2011, **3**, 1632

www.rsc.org/nanoscale

PAPER

A cationic surfactant assisted selective etching strategy to hollow mesoporous silica spheres†

Xiaoliang Fang, Cheng Chen, Zhaohui Liu, Pengxin Liu and Nanfeng Zheng*

Received 22nd November 2010, Accepted 18th December 2010
DOI: 10.1039/c0nr00893a

Hollow mesoporous silica spheres have recently attracted increasing attention. However, effective synthesis of uniform hollow mesoporous spheres with controllable well-defined pore structures for fundamental research and practical applications has remained a significant challenge. In this work, a straightforward and effective "cationic surfactant assisted selective etching" synthetic strategy was developed for the preparation of high-quality hollow mesoporous silica spheres with either wormhole-like or oriented mesoporous shell. The as-prepared hollow mesoporous silica spheres have large surface area, high pore volume, and controllable structure parameters. Our experiments demonstrated that cationic surfactant plays critical roles in forming the hollow mesoporous structure. A formation mechanism involving the etching of solid SiO_2 accelerated by cationic surfactant followed by the redeposition of dissolved silica species directed by cationic surfactant is proposed. Furthermore, the strategy can be extended as a general strategy to transform silica-coated composite materials into yolk-shell structures with either wormhole-like or oriented mesoporous shell.

Introduction

Design and synthesis of hollow micro-/nanostructures have been intensively pursued in the past decade.[1–4] As a special type of these materials, hollow mesoporous silica spheres (HMSS) have attracted increasing attention especially in drug delivery and confined catalysis because of their several fascinating properties such as large surface area, excellent mechanical and thermal stability, low toxicity, high biocompatibility, high drug loading capacity, and highly permeable porous shell for easy loading and release of guest species.[5–9] In previous studies, the most widely used strategies for synthesis of HMSS are hard-template[10–16] and soft-template[17–23] methods. The hard-template method was typically processed in multiple steps including the fabrication of sacrificial hard templates and their surface functionalization followed by the deposition of mesoporous silica shell and selective etching of the core templates. When uniform inorganic or polymer beads are used as sacrificial templates, although it is possible to obtain highly uniform HMSS, the required multi-step procedures are, in general, time-consuming and somewhat cumbersome. On the other hand, the soft-template method using micelle and vesicles reduces working procedure of the after-treatment, though the synthesis of the soft templates themselves may require complex procedures. Nevertheless, because of the difficulty in maintaining the uniformity of the soft templates in solution, the size distribution for HMSS made by the soft-template method is typically poor. Consequently, facile synthetic routes to high-quality HMSS are desirable for their practical applications.

Very recently, new synthetic methods based on a silica-based etching strategy have been successfully developed to fabricate uniform HMSS and rattle-type mesoporous silica spheres. In these reported methods, solid silica spheres or modified solid silica spheres were used as the templates to create HMSS by selectively etching out the interior silica.[9,24–29]

As compared with other methods, such a selective etching strategy is facile and economical. Unfortunately, due to the lack of an effective way to control the pore formation, the pores in the HMSS particles obtained by the reported selective etching strategy were usually disordered and broadly distributed.[9,24–29] However, for many applications of mesoporous silica materials, ordered and narrow-distributed pores are critical. For example, many recent reports have demonstrated that the chemical modification of the uniform pores in MCM-41 type materials can be used to regulate drug release and even fabricate controllable drug-release nanodevices.[30–33] Therefore, from the viewpoint of both fundamental research and practical applications, there is

State Key Laboratory for Physical Chemistry of Solid Surfaces and Department of Chemistry, College of Chemistry and Chemical Engineering, Xiamen University, Xiamen, 361005, China. E-mail: nfzheng@xmu.edu.cn

† Electronic supplementary information (ESI) available: Experimental procedures for $s$$SiO_2$ with different sizes, α-Fe_2O_3@HMSS-W, α-Fe_2O_3@HMSS-O, Au@HMSS-W, and Au@HMSS-O; SEM images of HMSS-W; the histogram of size distribution of $s$$SiO_2$ and HMSS-W; TEM images and the corresponding pore size distributions of HMSS-W obtained by using the CTAC/C_{12}TAB; TEM images of HMSS-W obtained by using the $s$$SiO_2$ with particle sizes of 470 nm; TEM images of the product obtained by using the 10 mg mL^{-1} CTAB in the synthetic procedure of HMSS-W; SEM images of HMSS-O; TEM images of Au@SiO_2, Au@HMSS-W, Au@SiO_2@CTAB/SiO_2, and Au@HMSS-O. See DOI: 10.1039/c0nr00893a

a significant need to develop facile and effective strategies for preparing uniform HMSS with controllable well-defined pore structures.

In this study, we report a straightforward and effective "cationic surfactant assisted selective etching" (CSASE) route to high-quality HMSS with either wormhole-like or oriented mesoporous shell. Simply by treating solid SiO_2 spheres with a Na_2CO_3 solution in the presence of a cationic surfactant (*i.e.* CTAB), HMSS particles with wormhole-like shell (denoted as HMSS-W) were easily prepared. By investigating the roles of CTAB, we proposed an etching-redeposition mechanism for the formation of HMSS-W from the solid SiO_2 spheres and revealed the importance of CTAB in stabilizing CTAB/SiO_2 mesostructures from alkaline etching. Such understanding was then used to prepare HMSS particles with oriented mesoporous shell (denoted as HMSS-O) by selectively etching the solid SiO_2 core from the pre-made core-shell SiO_2@CTAB/SiO_2 spheres with oriented mesoporous structure. The pore channels in HMSS-O are aligned perpendicularly to the surface of spheres. By using CTAB as the template, the pores in both HMSS-W and HMSS-O are narrowly distributed around 2.5 nm. More importantly, the synthetic strategy developed in this work can be extended to fabricate yolk-shell nanostructures with functional nanoparticles encapsulated in HMSS, making the strategy useful and widely applicable for preparing advanced mesoporous materials for catalysis and drug delivery.

Experimental

Chemicals

Tetraethyl orthosilicate (TEOS) was purchased from Alfa Aesar. Ammonia solution (25–28%), cetyltrimethyl ammonium bromide (CTAB), cetyltrimethyl ammonium chloride (CTAC), ethanol, acetone, and sodium carbonate were purchased from Sinopharm Chemical Reagent Co. (Shanghai, China). Dodecyltrimethylammonium bromide (C_{12}TAB) was purchased from TCI (Shanghai) Development Co., Ltd. All the reagents were used without further purification. Deionized water was used in all experiments.

Synthesis of solid SiO_2 spheres (denoted as *s*SiO_2)

sSiO_2 were synthesis following a modified Stöber method. In a typical synthesis, 6 mL of TEOS were rapidly added into a mixture of ethanol (74 mL), deionized water (10 mL), and ammonium aqueous solution (25–28%, 3.15 mL). The mixture was then stirred at room temperature for 1 h, resulting in the formation of a white silica colloidal suspension. The silica particles were centrifugally separated from the suspension and washed with deionized water and ethanol.

Synthesis of HMSS-W

50 mg of the as-prepared *s*SiO_2 were homogeneously dispersed in 9 mL of deionized water by ultrasonication for 15 min. After the addition of 1 mL CTAB aqueous solution (12.5 mg mL^{-1}), the resultant mixture was further stirred at room temperature for 30 min before the introduction of Na_2CO_3 (212 mg). After the reaction was stirred at 35 °C for 24 h, the products were collected by centrifugation and washed with deionized water and ethanol.

Synthesis of *s*SiO_2@CTAB/SiO_2

50 mg of the as-prepared *s*SiO_2 was homogeneously dispersed in 10 mL of deionized water by ultrasonication for 15 min. The suspension was then added into a solution containing CTAB (75 mg), deionized water (15 mL), ethanol (15 mL), and ammonia solution (0.275 mL). After the mixture was stirred at room temperature for 0.5 h, 0.125 mL of TEOS was added quickly. After the reaction with stirring for 6 h, the products were collected by centrifugation, and redispersed in 10 mL of deionized water.

Synthesis of HMSS-O

With vigorous stirring, 212 mg of Na_2CO_3 were added into the well-sonicated water suspension of the above *s*SiO_2@CTAB/SiO_2. After the reaction was stirred at 50 °C for 10 h, the products were collected by centrifugation and extensively washed with deionized water and ethanol.

Removal of CTAB from the as-prepared products

Calcination or extraction was used to remove CTAB from the as-prepared products. For the calcination process, the as-prepared products were heated to 550 °C in air at a rate of 1.5 °C min^{-1} and maintained for 6 h. For the extraction process, the as-prepared products were dispersed in 80 mL of acetone and refluxed at 80 °C for 48 h. The extraction was repeated three times to fully remove CTAB. The final products were collected and washed with deionized water. After removal of CTAB, the sample *s*SiO_2@CTAB/SiO_2 was designated as *s*SiO_2@*m*SiO_2.

Characterization

Scanning electron microscopy (SEM) and transmission electron microscopy (TEM) images were taken on a Hitachi S-4800 microscope with a field-emission electron gun and a TECNAI F-30 high-resolution transmission electron microscope operating at 300 kV, respectively. To prepare samples for SEM or TEM observations, one drop of ethanol suspension was deposited onto either silicon wafer (for SEM) or carbon-coated copper grid (for TEM). The structure of the products was also characterized by X-ray powder diffraction (XRD, Panalytical X'pert PRO diffractometer with Cu Kα radiation). The surface area was measured by the Brunauer–Emmett–Teller (BET) method using nitrogen adsorption and desorption isotherms on a Micrometrics ASAP 2020 system. The pore size distribution plot was obtained by the Barrett–Joyner–Halenda (BJH) method. The zeta potentials were measured on Nano-ZS (Malvern). The pH of the solutions was recorded with pH meter S20 (Mettler Toledo).

Results and discussion

Facile conversion of *s*SiO_2 into uniform HMSS-W

When simply treated by Na_2CO_3 in the presence of CTAB in an appropriate concentration, as illustrated in Fig. 1, the solid Stöber spheres were successfully converted into uniform hollow

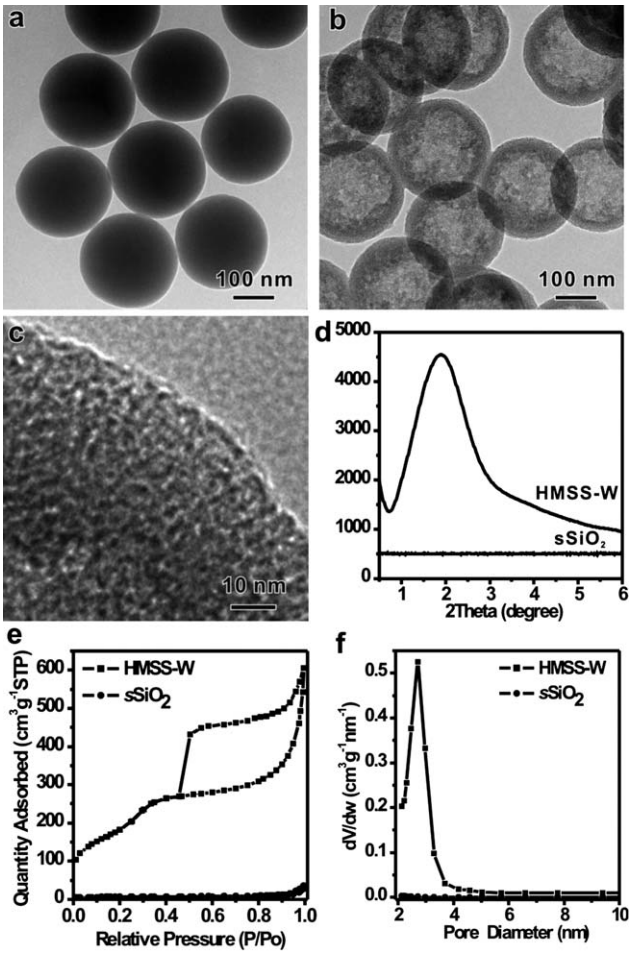

Fig. 1 TEM images: (a) sSiO$_2$, (b, c) HMSS-W, (d) low-angle X-ray diffraction pattern of sSiO$_2$ and HMSS-W, and (e, f) N_2 sorption isotherms and the pore size distribution of sSiO$_2$ and HMSS-W.

spheres (see Fig. S1 for the SEM images†). As revealed by the high-magnification TEM image (Fig. 1c), the shell of the as-obtained HMSS displays an obvious wormhole-like mesoporous structure. The mesostructure in HMSS-W was further confirmed by the powder X-ray diffraction (XRD). While the original sSiO$_2$ does not diffract at low angles, the as-prepared HMSS-W exhibits a definite diffraction peak at 2.1° (2θ) with a weak and broad shoulder peak around 3.9°, which is typical of the wormhole mesostructures. The rather thin and curved feature of the mesoporous shell and therefore small diffraction domains might also account for the relatively broad primary peak and absence of well-defined high-order diffraction peaks.[12] After thermal calcination to remove CTAB, the porosity of HMSS-W was investigated by N_2 adsorption-desorption measurements. As shown in Fig. 1f, the calcined HMSS-W exhibits a type IV isotherm with a type H2 hysteresis loop, characteristic of mesoporous materials. The BET surface area and pore volume of HMSS-W are 669.0 m^2 g^{-1} and 0.97 cm^3 g^{-1}, respectively. In comparison, the BET surface area of sSiO$_2$ is only 22.0 m^2 g^{-1}. As revealed by the pore size distribution of HMSS-W obtained from the analysis of the adsorption branch of the isotherm using the BJH method, HMSS-W has a rather narrow size distribution centered at 2.5 nm, similar to that of MCM-41. We thus believe that the pore formation in the HMSS-W is related to CTAB.

Roles of CTAB in the formation of HMSS-W

In order to understand the essential role of the CTAB in the formation of HMSS-W, a series of experiments were carried out by varying the CTAB concentration while keeping all other reaction conditions the same. Surprisingly, no hollow spheres were obtained in the absence of CTAB (Fig. 2a). Although the surface of sSiO$_2$ became slightly rough, no significant size shrinking of sSiO$_2$ was observed either, indicating that the etching process of sSiO$_2$ caused by Na_2CO_3 alone was negligible. The alkaline etching of silica by Na_2CO_3 was considerably accelerated by the presence of CTAB. When CTAB was present in a concentration of 0.1 mg mL^{-1}, sSiO$_2$ were converted into core-shell spheres with a solid core and a thin layer of disordered mesoporous shell (Fig. 2b). The average diameter of the yolk was 200 nm, smaller than that of the unetched sSiO$_2$ (245 nm). This size reduction gave evidence to the fact that CTAB promoted the etching of sSiO$_2$ by Na_2CO_3. However, what was the reason behind such a promotion? The simultaneous formation of disordered mesoporous shell during the etching process provided us with some hints to solve this puzzle. At the CTAB concentration of 0.1 mg mL^{-1}, the outer mesoporous shell was rather thin and even discontinuous. When the CTAB concentration was increased to 0.3 mg mL^{-1}, a continuous mesoporous shell with an average thickness of 13 nm was completely formed on all particles while the core was further etched out (Fig. 2c). Careful observation also revealed that the more the yolk was etched, the thicker was the porous shell. When the CTAB concentration was

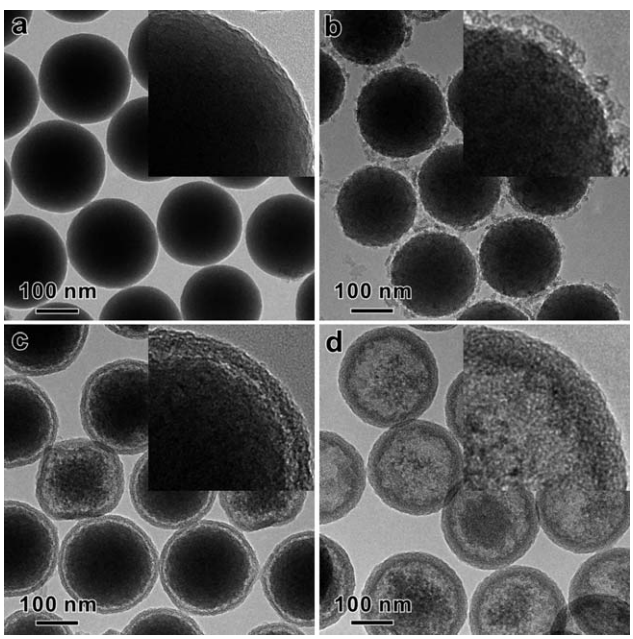

Fig. 2 TEM images show the effect of CTAB concentration on the conversion of sSiO$_2$ to HMSS. The CTAB concentration used were (a) 0 mg mL^{-1}, (b) 0.1 mg mL^{-1}, (c) 0.3 mg mL^{-1}, and (d) 0.6 mg mL^{-1}. All the other reaction conditions are the same: 50 mg sSiO$_2$, 212 mg Na_2CO_3, 35 °C for 24 h. Shown in the inset are the corresponding TEM image with higher magnification.

further increased to 0.6 mg mL^{-1}, the etching degree of the core was further extended and the thickness of mesoporous shell was increased to about 25 nm (Fig. 2d). If 1.25 mg mL^{-1} CTAB was used, all solid spheres were eventually converted into HMSS with the core extensively etched out after the 24 h reaction. The thickness of the porous shell was measured to be 40 nm (Fig. 1).

In the absence of CTAB, no obvious etching of the sSiO$_2$ was observed. The etching process was significantly accelerated by the use of CTAB and a higher CTAB concentration yielded a thicker mesoporous shell before the depletion of the sSiO$_2$. This observation clearly implies that the etching promotion effect by CTAB is essentially driven by the redeposition of dissolved silica species assisting by CTAB. Therefore, in the conversion process of sSiO$_2$ to HMSS, CTAB should at least play the following two important roles: 1) the soft template to direct the formation of the mesoporous structure in the shell by co-assembly with the dissolved silica species; 2) the promoter to drive the dissolution dynamics of the sSiO$_2$ and therefore accelerate their etching.

Formation mechanism of HMSS-W

Based on the above discussion over the roles of CTAB, we propose in Scheme 1 a formation mechanism of HMSS-W from sSiO$_2$. Three important processes are involved in the conversion of sSiO$_2$ into the hollow mesoporous structure: 1) adsorption of CTAB on the surface of sSiO$_2$, 2) slow dissolution of SiO$_2$ in the alkaline solution to form soluble silicate species, and 3) co-assembly of CTAB with soluble silicate species to form the mesostructure.

Under the conditions of our procedure (35 °C, pH = 10.7), the dissolution of sSiO$_2$ by Na$_2$CO$_3$ alone is very slow. However, at this pH, the sSiO$_2$ spheres are negative charged, thereby benefiting the adsorption of cetyltrimethylammonium cations (CTA^+) on their surface. As evidenced by zeta-potential measurements (Fig. 3), the adsorption of CTA^+ makes the sSiO$_2$ spheres positively charged with a zeta-potential of 4.0 mV. Since the silicate species etch-released from sSiO$_2$ are anionic, the positive charge of the CTA^+-adsorbing sSiO$_2$ surface helps the re-deposition of the soluble silicate. Such a silicate redeposition process consumes some released silicate species and thus

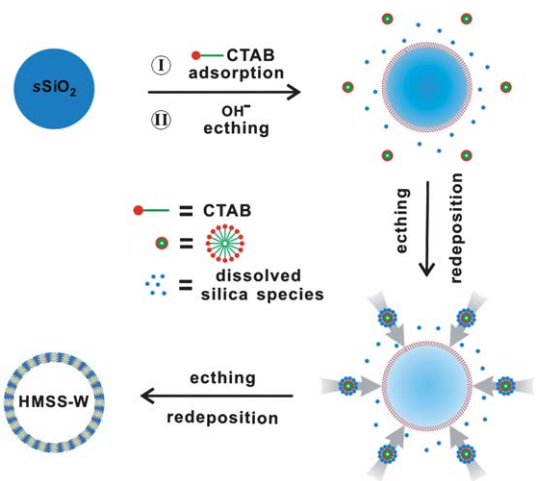

Scheme 1 Schematic illustration for the formation of HMSS-W.

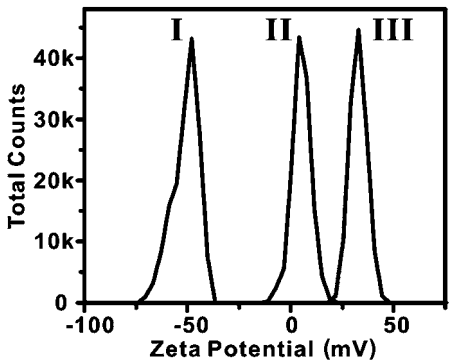

Fig. 3 The distribution of zeta potentials of sSiO$_2$ (I), CTAB-adsorbing sSiO$_2$ (II), and HMSS-W (III).

kinetically drives the dissolution reaction of sSiO$_2$. More importantly, the redeposition of the etched-out silicate allows more adsorption of CTA^+ (Fig. 3) and eventually leads to the formation of the mesostructured CTAB/SiO$_2$ shell on the surface of sSiO$_2$ spheres. Such an CTA^+-promoted etching-redeposition formation mechanism is different from that involved in Yin's process.[24,25]

In order to demonstrate that soluble silicate species were indeed released from sSiO$_2$, we designed an elaborate experiment to capture some of the dissolved silicate species by adding non-silica particles (*i.e.* rice-like α-Fe$_2$O$_3$) into the synthesis procedure (Fig. 4a). At the end of the reaction, the formation of core-shell structure with the core of the rice-like α-Fe$_2$O$_3$ particle can be observed by SEM (Fig. 4b) and TEM (Fig. 4c). The elemental mapping by EDX analysis (Fig. 4d-f) confirms the presence of a silica layer on each α-Fe$_2$O$_3$ particle, suggesting that the released silicate species can be easily re-condensed to form silica network. The proposed etching-redeposition mechanism was also supported by the size measurements on the as-prepared HMSS-W spheres. According to the mechanism, the initial co-assembly deposition of CTA^+ with silicate released from the core occurred on the surface of the original sSiO$_2$. Therefore, one would predict that the outer diameter of HMSS-W should be somewhat larger than the diameter of the original sSiO$_2$. Indeed, starting from sSiO$_2$, with an average diameter of 245 ± 10 nm (Fig. S2†), the outer diameter of the obtained HMSS-W was measured to be 260 ± 10 nm (Fig. S2†).

Considering that the essential role of CTAB during the formation of HMSS-W comes from the CTA^+ cations, it was expected that the conversion of sSiO$_2$ into HMSS-W could also be achieved by replacing CTAB with other quaternary cationic surfactants. Indeed, for instance, HMSS-W particles were also successfully prepared from sSiO$_2$ by replacing CTAB with CTAC (Fig. S3†). When CTAB was substituted with C_{12}TAB, hollow mesoporous spheres were successfully obtained. The pore size of the resultant HMSS was 2.1 nm, smaller than that of HMSS made by CTAB (Fig. S3†). By varying the size of cationic surfactants or using pore swelling agents, the CSASE strategy reported here should provide an effective method to create HMSS-W with tunable pore size over a wide range. Furthermore, the size of HMSS-W is also tunable by simply varying the size of the sSiO$_2$ template. For instance, by the same surfactant-assisted etching procedures, the HMSS-W with particle sizes of

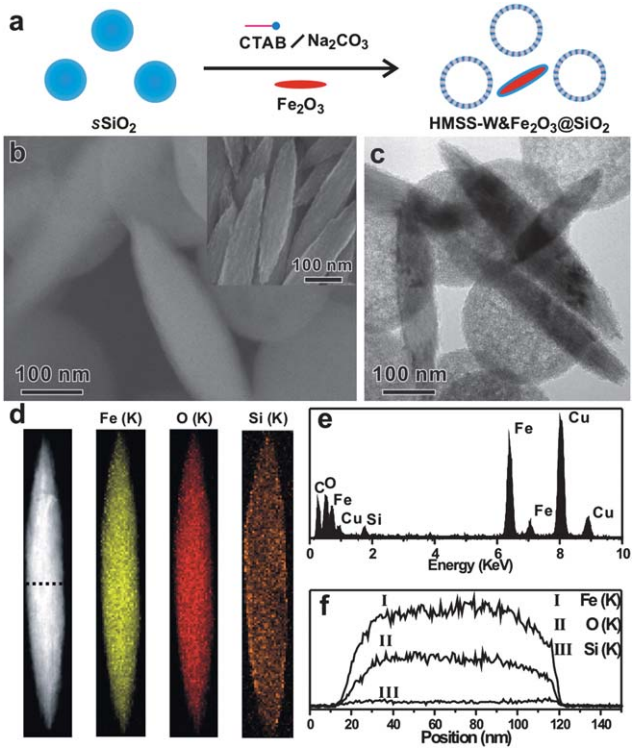

Fig. 4 (a) Schematic illustration of capturing dissolved silicate species by rice-like α-Fe_2O_3 particles, (b, c) SEM and TEM images of as-obtained products (inset: SEM image of rice-like α-Fe_2O_3 particles), (d, e, and f) characterization of as-obtained single core-shell particle: (d) mapping of elements by EDX analysis under the STEM mode, (e) integrated EDX spectrum (the Cu signals are attributed to the TEM grid of copper used for the EDX experiments), (f) EDX line scanning profile.

490 nm is obtained simply by using the $s$$SiO_2$ with particle sizes of 470 nm (Fig. S4†).

Formation of HMSS with oriented mesoporous shell

For many applications, mesoporous materials with through pores running perpendicularly to their surface are highly desirable. Particularly for catalysis applications, such a pore structure would significantly shorten the diffusion length of target molecules and therefore enhance their overall catalytic performance. Unfortunately, the mesopores of the HMSS obtained by the one-step etching-redeposition strategy discussed above were wormhole-like. According to previous studies, the use of increased concentration of surfactant is important to obtain an ordered mesostructure rather than a wormhole-like mesostructure.[36] We therefore increased the CTAB concentration to 10 mg mL^{-1} in our synthesis. However, no formation of hollow spheres with continuous mesoporous shell was observed. The reaction yielded smaller mesoporous silica particles surrounding the large SiO_2 particles, which can be explained by the burst nucleation of a large number of small mesoporous silica particles on the surface of $s$$SiO_2$ induced by the increased CTAB concentration (Fig. S5†). This result indicates the difficulty involved in the one-step conversion of $s$$SiO_2$ into HMSS with mesopores oriented perpendicular to their surface.

On the basis of the observation that the silicate-CTAB mesostructured shell of HMSS-W was fairly stable against the alkaline etching, we have switched to a two-step process to convert solid $s$$SiO_2$ into HMSS with oriented pore structure. In this process, core-shell spheres $s$$SiO_2$@CTAB/$SiO_2$ with ordered mesoporous shell with perpendicular pores were first made. The solid SiO_2 cores of the as-prepared $s$$SiO_2$@CTAB/$SiO_2$ were then selectively etched out by Na_2CO_3 to create the hollow spheres. In our experiments, the $s$$SiO_2$@CTAB/$SiO_2$ particles were prepared using modified literature methods.[34,35] As clearly revealed by TEM (Fig. 5), the mesopores within the shell (about 50 nm in thickness) of the as-prepared $s$$SiO_2$@CTAB/$SiO_2$ were nicely oriented perpendicular to the surface of the spheres. As expected, after the alkaline treatment, the inner solid SiO_2 core of each $s$$SiO_2$@CTAB/$SiO_2$ sphere was completely etched out while its outer shell remained intact, resulting in the formation of HMSS-O (see Fig. S6 for the SEM images†) with an oriented pore structure. As observed in the shell of the unetched $s$$SiO_2$@CTAB/$SiO_2$

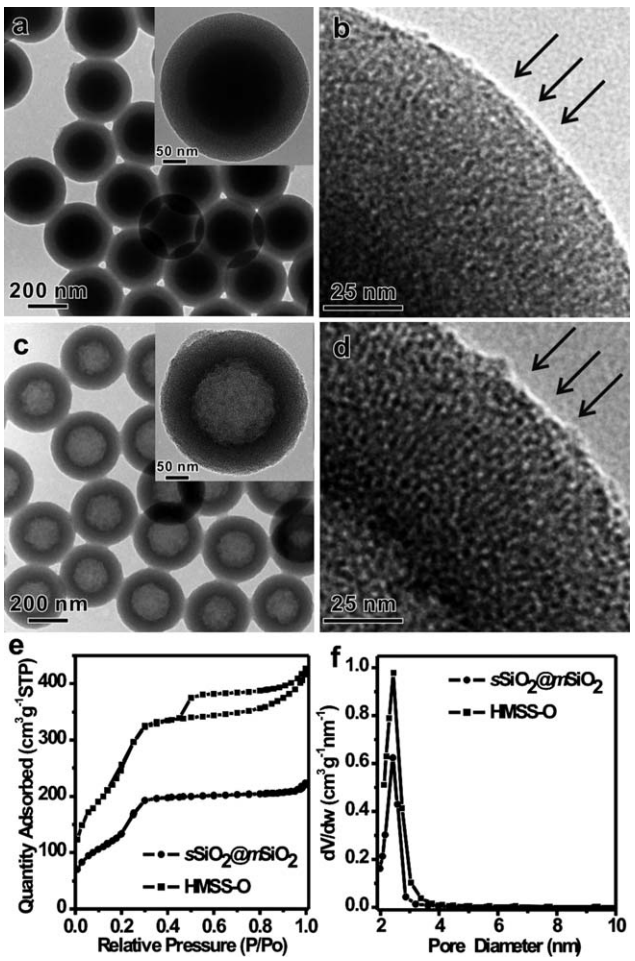

Fig. 5 (a) TEM image of as-prepared $s$$SiO_2$@CTAB/$SiO_2$ (inset: typical TEM image of a single $s$$SiO_2$@CTAB/$SiO_2$ particle), (b) high-magnification TEM image corresponding to the dashed pane in inset of (a), (c) TEM image of as-prepared HMSS-O (inset: typical TEM image of single HMSS-O particle), (d) high-magnification TEM image corresponding to the dashed pane in inset of (c), and (e, f) N_2 sorption isotherm and the pore size distribution of $s$$SiO_2$@$m$$SiO_2$ and HMSS-O. The orientation of the mesopores is indicated by arrows.

spheres, all mesopore channels in HMSS-O were perpendicular to the surface of the spheres (indicated by arrows). After calcination, the BET surface area and pore volume of HMSS-O were measured to be 937 $m^2 g^{-1}$ and 0.77 $cm^3 g^{-1}$, respectively. In comparison, the calcined sSiO$_2$@CTAB/SiO$_2$ sample (sSiO$_2$@mSiO$_2$) had a BET surface area of 493 $m^2 g^{-1}$ and a pore volume of 0.41 $cm^3 g^{-1}$.

The successful synthesis of HMSS-O from sSiO$_2$@CTAB/SiO$_2$ further confirms that, under the alkaline etching conditions, the CTAB/SiO$_2$ mesostructure is more stable than the solid SiO$_2$ core. Very recently, Shi's group also reported a better stability of mesostructured organic-containing silica shell made from TEOS and octadecyltrimethoxysilane.[26] Based on ^{29}Si MAS NMR studies, they attributed the better stability of the mesostructured shell to the higher degree of condensation in the mesoporous shell than in the solid core. But in our case of sSiO$_2$@CTAB/SiO$_2$, we hypothesized that the better stability of the CTAB/SiO$_2$ mesostructure was mainly due to the presence of CTAB surfactant in the composite. Based on this hypothesis, a different result was expected if CTAB was removed from the CTAB/SiO$_2$ mesostructured shell before alkaline etching. Therefore, in a control experiment, we removed CTAB extensively by acetone extraction. The obtained sSiO$_2$@mSiO$_2$ spheres were then subjected to alkaline etching by Na_2CO_3 at 50 °C. As shown in Fig. 6, no formation of HMSS was observed. After etching for 1 h, the mesoporous shell of sSiO$_2$@mSiO$_2$ spheres was heavily etched to form a disordered mesoporous shell but the solid core was only slightly etched (Fig. 6a). Upon increasing the etching time to 2 h, the mesoporous shell of sSiO$_2$@mSiO$_2$ spheres entirely disappeared and the diameter of the solid core decreased (Fig. 6b). This result reinforces our hypothesis that the presence of CTAB is the most important factor to stabilize the silicate-CTAB shell against alkaline etching.

It is worth noting that the structure parameters of core-shell spheres sSiO$_2$@CTAB/SiO$_2$, such as the shell thickness and the core size, could be precisely tuned by varying the amount and the initial sizes of solid SiO$_2$ core during the synthetic procedure (see Supporting Information†). As shown in Fig. 7a and b, by simply changing the initial amount of sSiO$_2$, the shell thickness of core-shell spheres sSiO$_2$@CTAB/SiO$_2$ can be tuned to 100 nm. After the alkaline etching, the wall thickness of as-obtained HMSS-O is about 100 nm, meanwhile keeping the pore orientation perpendicular to the surface. HMSS-O with hollow interior sizes of 470 nm (Fig. 7c, d) and 130 nm (Fig. 7e and f) were obtained simply by using the sSiO$_2$ with particle sizes of 470 nm and 130 nm as the templates for synthesis of sSiO$_2$@CTAB/SiO$_2$.

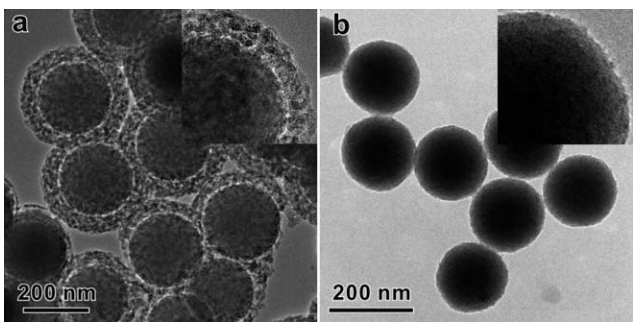

Fig. 6 TEM image of sSiO$_2$@mSiO$_2$ etched by Na_2CO_3 for 1 h (a) and 2 h (b), inset: typical high-magnification TEM images.

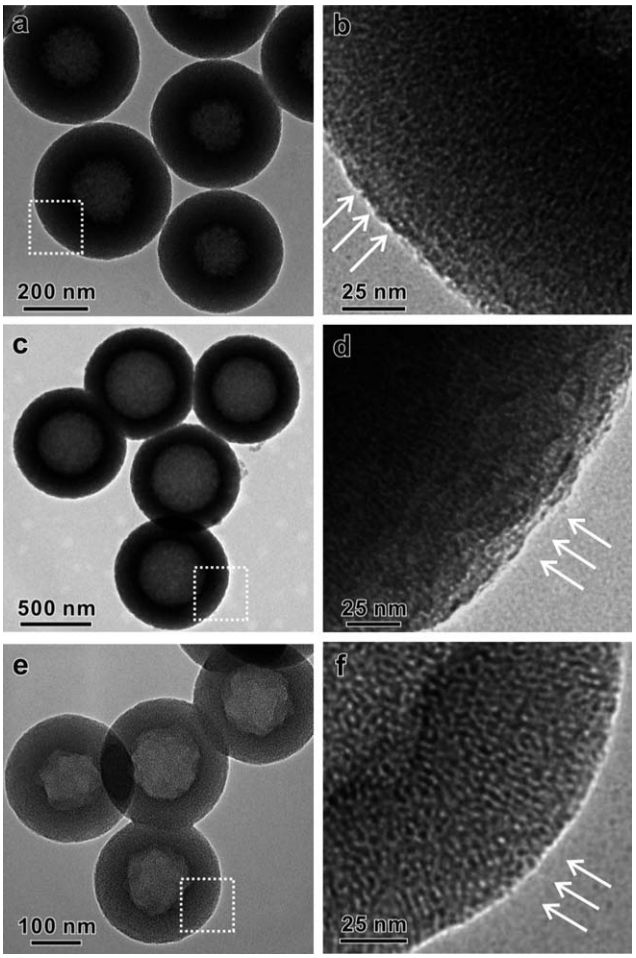

Fig. 7 TEM characterization of HMSS-O with different structure parameters: (a) HMSS-O with wall thickness of 100 nm, (b) high-magnification TEM image corresponding to the dashed pane in inset of (a), (c) HMSS-O with hollow interior size of 470 nm, (d) high-magnification TEM image corresponding to the dashed pane in inset of (c), (e) HMSS-O with hollow interior size of 130 nm, (f) high-magnification TEM image corresponding to the dashed pane in inset of (e). Oriented mesopores are indicated by arrows.

Preparation of yolk-shell particles with wormhole-like/oriented mesoporous shell

Yolk-shell structures with individual nanocrystals encapsulated in hollow porous particles have been recently demonstrated not only to effectively enhance the stability of nanocrystals for catalysis applications, but also to introduce more functionality for bio-applications.[37–39] Such yolk-shell structures were commonly fabricated by coating silica-encapsulated nanocrystals with a layer of porous material followed by selective etching of silica.[8,9,26,37] As described above, the CSASE strategy that we have developed in this study has significantly simplified the direct conversion of sSiO$_2$ into hollow mesoporous structures. We were therefore intrigued to explore the possibility of using such a simplified method for the preparation of yolk-shell particles with mesoporous shells. To further demonstrate the effectiveness of the developed CSASE strategy in converting non-spherical SiO$_2$ particles, ellipsoid-shaped α-Fe$_2$O$_3$@SiO$_2$

core-shell particles were prepared for the demonstration. As shown in Fig. 8a–c, after 24 h etching by Na_2CO_3 in the presence of CTAB at 35 °C, all of the α-Fe_2O_3@SiO_2 core-shell particles were converted into elliptical yolk-shell particles with the ellipsoid-shaped α-Fe_2O_3 yolk nicely encapsulated inside. Similar to HMSS-W prepared from *s*SiO_2 in one-step, the mesopores in the obtained elliptical SiO_2 shell were wormhole-like. When the two-step protocol was used for transformation of the ellipsoid-shaped α-Fe_2O_3@SiO_2, we obtained elliptical yolk-shell particles with ordered mesoporous shell with pores oriented perpendicular to their surface (Fig. 8d–f). Such an oriented porous structure is similar to that observed for HMSS-O prepared using the two-step method. Furthermore, when using Au@SiO_2 core-shell nanospheres to replace *s*SiO_2, Au@SiO_2 yolk-shell structures with either wormhole-like or oriented mesoporous shells can also be successfully obtained *via* the proposed CSASE strategy (Fig. S7†). Based on these results, we believe that the CSASE strategy reported here is applicable to the synthesis of yolk-shell nanostructures with diverse compositions, structures and functions.

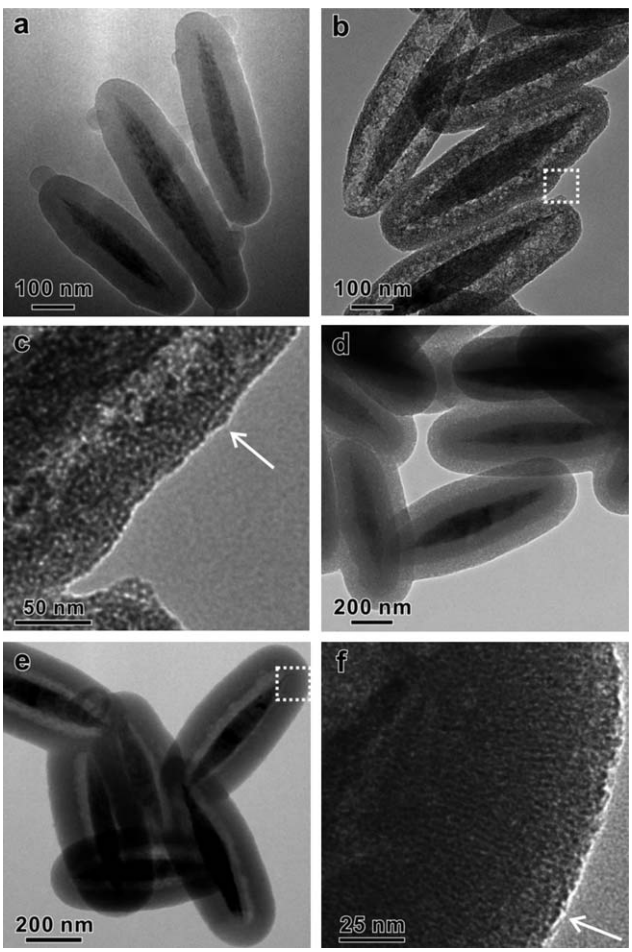

Fig. 8 (a) TEM image of ellipsoid-shaped α-Fe_2O_3@SiO_2, (b, c) TEM images of ellipsoid-shaped α-Fe_2O_3@HMSS-W, (d) TEM image of ellipsoid-shaped α-Fe_2O_3@SiO_2@CTAB/SiO_2, and (e, f) TEM images of ellipsoid-shaped α-Fe_2O_3@HMSS-O. Oriented mesopores are indicated by arrows.

Conclusions

In summary, we have developed a facile route to fabricate hollow mesoporous silica with a wormhole-like shell based on a CSASE strategy. The use of cationic surfactant is critical to the formation of the hollow mesoporous structure from *s*SiO_2. The surfactant plays the following three important roles in the reported solid to hollow transformation process: 1) a soft template to direct the formation of the mesoporous structure in the shell, 2) a promoter to accelerate etching of *s*SiO_2 (*i.e.* hard-template), 3) a stabilizer to protect the silicate-CTAB shell from alkaline etching. On the basis of such understanding of roles of the cationic surfactant, we have successfully converted solid *s*SiO_2 into hollow mesoporous silica with oriented mesoporous structure by selectively etching the pre-made core-shell *s*SiO_2@CTAB/SiO_2 composite with oriented mesoporous structure. Such a CSASE strategy is remarkably effective and reproducible, providing a facile route to tailor the structure parameters of as-obtained HMSS by selecting the appropriate cationic surfactant and also *s*SiO_2 template. Furthermore, the strategy can be extended as a general strategy to transform silica-coated composite materials into yolk-shell structures with either wormhole-like or oriented mesoporous shell. We thus believe that the strategy reported herein will stimulate chemists to explore its further promising applications, such as confined catalysis and controlled release.

Acknowledgements

We thank NSFC (21021061, 20925103, 20923004, 20871100), MOST of China (2009CB930703, 2011CB932403), the Fok Ying Tung Education Foundation (121011), NSF of Fujian for a Distinguished Young Investigator Grant (2009J06005) and the Key Scientific Project of Fujian Province (2009HZ0002-1).

Notes and references

1 F. Caruso, R. A. Caruso and H. Möhwald, *Science*, 1998, **282**, 1111–1114.
2 Y. G. Sun, B. Mayers and Y. N. Xia, *Adv. Mater.*, 2003, **15**, 641–646.
3 C. S. Peyratout and L. Dähne, *Angew. Chem., Int. Ed.*, 2004, **43**, 3762–3783.
4 X. W. Lou, L. A. Archer and Z. C. Yang, *Adv. Mater.*, 2008, **20**, 3987–4019.
5 L. Du, S. J. Liao, H. A. Khatib, J. F. Stoddart and J. I. Zink, *J. Am. Chem. Soc.*, 2009, **131**, 15136–15142.
6 Y. F. Zhu, T. Ikoma, N. Hanagata and S. Kaskel, *Small*, 2010, **6**, 471–478.
7 Y. F. Zhu, J. L. Shi, W. H. Shen, H. R. Chen, X. P. Dong and M. L. Ruan, *Nanotechnology*, 2005, **16**, 2633–2638.
8 Q. Zhang, T. R. Zhang, J. P. Ge and Y. D. Yin, *Nano Lett.*, 2008, **8**, 2867–2871.
9 J. Lee, J. C. Park, J. U. Bang and H. Song, *Chem. Mater.*, 2008, **20**, 5839–5844.
10 B. Tan and S. E. Rankin, *Langmuir*, 2005, **21**, 8180–8187.
11 F. J. Suárez, M. Sevilla, S. Álvarez, T. Valdés-Solís and A. B. Fuertes, *Chem. Mater.*, 2007, **19**, 3096–3098.
12 H. Blas, M. Save, C. P.PasettoBoissière, C. Sanchez and B. Charleux, *Langmuir*, 2008, **24**, 13132–13137.
13 W. R. Zhao, M. D. Lang, Y. S. Li, L. Li and J. L. Shi, *J. Mater. Chem.*, 2009, **19**, 2778–2783.
14 Y. F. Zhu, E. Kockrick, T. Ikoma, N. Hanagata and S. Kaskel, *Chem. Mater.*, 2009, **21**, 2547–2553.
15 Y. Yamada, M. Mizutani, T. Nakamura and K. Yano, *Chem. Mater.*, 2010, **22**, 1695–1703.
16 G. G. Qi, Y. B. Wang, L. Estevez, A. K. Switzer, X. N. Duan, X. F. Yang and E. P. Giannelis, *Chem. Mater.*, 2010, **22**, 2693–2695.

17 C. E. Fowler, D. Khushalani and S. Mann, *Chem. Commun.*, 2001, 2028–2029.
18 J. G. Wang, Q. Xiao, H. J. Zhou, P. C. Sun, Z. Y. Yuan, B. H. Li, D. T. Ding, A. C. Shi and T. H. Chen, *Adv. Mater.*, 2006, **18**, 3284–3288.
19 M. H. Yu, H. N. Wang, X. F. Zhou, P. Yuan and C. Z. Yu, *J. Am. Chem. Soc.*, 2007, **129**, 14576–14577.
20 Z. G. Feng, Y. S. Li, D. C. Niu, L. Li, W. R. Zhao, H. R. Chen, L. Li, J. H. Gao, M. L. Ruan and J. L. Shi, *Chem. Commun.*, 2008, 2629–2631.
21 J. G. Wang, F. Li, H. J. Zhou, P. C. Sun, D. T. Ding and T. H. Chen, *Chem. Mater.*, 2009, **21**, 612–620.
22 J. Liu, S. B. Hartono, Y. G. Jin, Z. Li, G. Q. Lu and S. Z. Qiao, *J. Mater. Chem.*, 2010, **20**, 4595–4601.
23 X. J. Wu and D. S. Xu, *Adv. Mater.*, 2010, **22**, 1516–1520.
24 T. R. Zhang, J. P. Ge, Y. X. Hu, Q. Zhang, S. Aloni and Y. D. Yin, *Angew. Chem., Int. Ed.*, 2008, **47**, 5806–5811.
25 T. R. Zhang, Q. Zhang, J. P. Ge, J. Goebl, M. W. Sun, Y. S. Yan, Y. S. Liu, C. L. Chang, J. H. Guo and Y. D. Yin, *J. Phys. Chem. C*, 2009, **113**, 3168–3175.
26 Y. Chen, H. R. Chen, L. M. Guo, Q. J. He, F. Chen, J. Zhou, J. W. Feng and J. L. Shi, *ACS Nano*, 2010, **4**, 529–539.
27 Q. Zhang, J. P. Ge, J. Goebl, Y. X. Hu, Z. D. Lu and Y. D. Yin, *Nano Res.*, 2009, **2**, 583–591.
28 M. Roca and A. J. Haes, *J. Am. Chem. Soc.*, 2008, **130**, 14273–14279.
29 M. Grzelczak, M. A. Correa-Duarte and L. M. Liz-Marzán, *Small*, 2006, **2**, 1174–1177.
30 B. G. Trewyn, I. I. Slowing, S. Giri, H. T. Chen and V. S. Y. Lin, *Acc. Chem. Res.*, 2007, **40**, 846–853.
31 S. Angelos, E. Johansson, J. F. Stoddart and J. I. Zink, *Adv. Funct. Mater.*, 2007, **17**, 2261–2271.
32 I. I. Slowing, B. G. Trewyn, S. Giri and V. S. Y. Lin, *Adv. Funct. Mater.*, 2007, **17**, 1225–1236.
33 B. G. Trewyn, S. Giri, I. I. Slowing and V. S. Y. Lin, *Chem. Commun.*, 2007, 3236–3245.
34 S. B. Yoon, J. Y. Kim, J. H. Kim, Y. J. Park, K. R. Yoon, S. K. Park and J. S. Yu, *J. Mater. Chem.*, 2007, **17**, 1758–1761.
35 Y. H. Deng, D. W. Qi, C. H. Deng, X. M. Zhang and D. Y. Zhao, *J. Am. Chem. Soc.*, 2008, **130**, 28–29.
36 N. Baccile, D. Grosso and C. Sanchez, *J. Mater. Chem.*, 2003, **13**, 3011–3016.
37 S. H. Liu and M. Y. Han, *Chem.–Asian J.*, 2010, **5**, 36–45.
38 A. Guerrero-Martínez, J. Pérez-Juste and L. M. Liz-Marzán, *Adv. Mater.*, 2010, **22**, 1182–1195.
39 J. Liu, S. Z. Qiao, S. B. Hartono and G. Q. Lu, *Angew. Chem., Int. Ed.*, 2010, **49**, 4981–4985.